Closing the Water Balance with Cosmic-ray Soil Moisture Measurements and Assessing Their Relation to Evapotranspiration in Two Semiarid Watersheds

Adam P. Schreiner-McGraw[1], Enrique R. Vivoni[1,2*], Giuseppe Mascaro[3], and Trenton E. Franz[4]

1. School of Earth and Space Exploration,
Arizona State University, Tempe, AZ, 85287.

2. School of Sustainable Engineering and the Built Environment,
Arizona State University, Tempe, AZ, 85287.

3. Julie Ann Wrigley Global Institute of Sustainability,
Arizona State University, Tempe, AZ, 85287.

4. School of Natural Resources,
University of Nebraska-Lincoln, Lincoln, NE, 68583.

Revised version submitted to *Hydrology and Earth System Sciences*
October 5, 2015

* *Corresponding author address:* Enrique R. Vivoni, School of Earth and Space Exploration and School of Sustainable Engineering and the Built Environment, Arizona State University, ISTB4, Building 75, Room 769, Tempe, AZ, 85287-6004, Tel: (480) 727-3575, email: vivoni@asu.edu.

Abstract

Soil moisture dynamics reflect the complex interactions of meteorological conditions with soil, vegetation and terrain properties. In this study, intermediate scale soil moisture estimates from the cosmic-ray neutron sensing (CRNS) method are evaluated for two semiarid ecosystems in the southwestern United States: a mesquite savanna at the Santa Rita Experimental Range (SRER) and a mixed shrubland at the Jornada Experimental Range (JER). Evaluations of the CRNS method are performed for small watersheds instrumented with a distributed sensor network consisting of soil moisture sensor profiles, an eddy covariance tower and runoff flumes used to close the water balance. We found a very good agreement between the CRNS method and the distributed sensor network (RMSE of 0.009 and 0.013 m^3/m^3 at SRER and JER) at the hourly time scale over the 19-month study period, primarily due to the inclusion of 5 cm observations of shallow soil moisture. Good agreement was also obtained in soil moisture changes estimated from the CRNS and watershed water balance methods (RMSE = 0.001 and 0.082 m^3/m^3 at SRER and JER), with deviations due to bypassing of the CRNS measurement depth during large rainfall events. Once validated, the CRNS soil moisture estimates were used to investigate hydrological processes at the footprint scale at each site. Through the computation of the water balance, we showed that drier-than-average conditions at SRER promoted plant water uptake from deeper soil layers, while the wetter-than-average period at JER resulted in percolation towards deeper soils. The CRNS measurements were then used to quantify the link between evapotranspiration and soil moisture at a commensurate scale, finding similar predictive relations at both sites that are applicable to other semiarid ecosystems in the southwestern U.S.

Keywords: watershed hydrology, soil moisture variability, evapotranspiration, land-atmosphere interactions, COSMOS, North American monsoon.

1. Introduction

Soil moisture is a key land surface variable that governs important processes such as the rainfall-runoff transformation, the partitioning of latent and sensible heat fluxes and the spatial distribution of vegetation in semiarid regions (e.g., Entekhabi, 1995; Eltahir, 1998; Vivoni, 2012). Semiarid watersheds with heterogeneous vegetation in the southwestern United States (Gibbens and Beck, 1987; Browning et al., 2014) exhibit variations in soil moisture that challenge our ability to quantify land-atmosphere interactions and their role in hydrological processes (Dugas et al., 1996; Small and Kurc, 2003; Scott et al., 2006; Gutiérrez-Jurado et al., 2013; Pierini et al., 2014). Moreover, accurate measurements of soil moisture over scales relevant to land-atmosphere interactions in watersheds are difficult to obtain. Traditionally, soil moisture is measured continuously at single locations using techniques such as time domain reflectometry and then aggregated in space using a number of methods (Topp et al., 1980; Western et al., 2002; Vivoni et al., 2008b). Soil moisture is also estimated using satellite-based techniques, such as passive or active microwave sensors (e.g., Kustas et al., 1998; Moran et al., 2000; Kerr et al., 2001; Bartalis et al., 2007; Narayan and Lakshmi, 2008; Entekhabi et al., 2010), but spatial resolutions are typically coarse and overpass times infrequent as compared to the spatiotemporal variability of soil moisture occurring within semiarid watersheds.

One approach to address the scale gap in soil moisture estimation is through the use of cosmic-ray neutron sensing (CRNS) measurements (Zreda et al., 2008, 2012) that provide soil moisture with a measurement footprint of several hectares (Desilets et al., 2010). Developments of the CRNS method have focused on understanding the processes affecting the measurement technique, for example, the effects of vegetation growth (Franz et al., 2013a; Coopersmith et al., 2014), atmospheric water vapor (Rosolem et al., 2013), soil wetting and drying (Franz et al., 2012a), and horizontal heterogeneity (Franz et al., 2013b). To date, the validation of the CRNS technique has been performed using single site measurements, spatial aggregations of different measurement locations, and particle transport models (Desilets et al., 2010; Franz et al., 2013b; Zhu et al., 2015). Distributed sensor networks measuring the water balance components of small watersheds and the spatial variability of soil moisture within a watershed offer the opportunity to test the accuracy of the CRNS method through multiple, independent approaches. For instance, the CRNS technique can be validated based upon the application of the watershed water balance, as performed for the eddy covariance (EC) technique often used to measure surface turbulent fluxes (Scott, 2010; Templeton et al., 2014). Once validated, CRNS soil moisture estimates can be used to apply the water balance equation in a continuous fashion with the aim of quantifying hydrological fluxes during storm and interstorm periods, including the occurrence of percolation to deeper soil layers or the transfer of water from the deeper vadose zone to the atmosphere.

An important advantage of the CRNS technique is that its measurement scale is comparable to the footprint of evapotranspiration (*ET*) measurements based on the EC technique, whose extent depends on wind speed and direction, atmospheric stability, and instrument and surface roughness heights (e.g., Hsieh et al., 2000; Kormann and Meixner, 2001; Falge et al., 2002). Furthermore, the relation between *ET* and soil moisture is an important parameterization in land surface models (e.g., Laio et al., 2001; Rodríguez-Iturbe and Porporato, 2004; Vivoni et al., 2008a) and, in most cases, has been investigated using EC measurements of *ET* and soil moisture observations at single sites. A number of studies, however, have shown that accounting for the spatial variability of land surface states is important to properly identify the linkage with EC measurements (e.g., Detto et al., 2006; Vivoni et al., 2010; Alfieri and Blanken, 2012). In other words, aggregated turbulent fluxes should be compared to spatially-averaged surface states obtained at commensurate measurement scales. As a result, CRNS soil moisture estimates could be useful to improve the characterization of the relation between evapotranspiration flux and soil moisture. To our knowledge, soil moisture estimates from the CRNS technique have not been used to study the hydrological processes occurring in small watersheds overlapping with the measurement footprint or for improving the parameterization of land surface models.

In this contribution, we study the soil moisture dynamics of small semiarid watersheds in Arizona and New Mexico instrumented with a cosmic-ray neutron sensor, an eddy covariance tower, a runoff flume and a network of soil moisture sensor profiles. The watersheds represent the heterogeneous vegetation and soil conditions observed in the Sonoran and Chihuahuan Deserts of the southwestern U.S. (Templeton et al., 2014; Pierini et al., 2014). We first compare the CRNS method with the distributed sensor network and estimates from a novel method based on closing the water balance at each site. Given the simultaneous observations during the study period (March 2013 to September 2014, 19 months), we quantify the variations in hydrological processes (e.g., infiltration, evapotranspiration, percolation) that differentially occur at each site in response to varying precipitation. Combining these measurement techniques also affords the capacity to construct and compare relationships between the spatially-averaged CRNS estimates and the spatially-averaged *ET* obtained from the EC method. To our knowledge, this is the first study where CRNS measurements are validated via two independent methods at the small watershed scale and used to make new inferences about watershed hydrological processes.

2. Study Areas and Datasets

2.1. Study Sites and Their General Characteristics

The two study sites are long-term experimental watersheds in semiarid ecosystems of the southwestern United States. Watershed monitoring began in 1975 at the Santa Rita Experimental

Range (SRER), located 45 km south of Tucson, Arizona, in the Sonoran Desert (Fig. 1), as described by Polyakov et al. (2010) and Scott (2010). Precipitation at the site varies considerably during the year, with 54% of the long-term mean amount (364 mm/yr) occurring during the summer months of July to September due to the North American monsoon (Vivoni et al., 2008a; Pierini et al., 2014). Soils at the SRER site are a coarse-textured sandy loam (Anderson, 2013) derived from Holocene-aged alluvium from the nearby Santa Rita Mountains. The savanna ecosystem at the site consists of the velvet mesquite tree (*Prosopis velutina* Woot.), interspersed with grasses (*Eragrostis lehmanniana*, *Bouteloua rothrockii*, *Muhlenbergia porteri* and *Aristida glabrata*) and various cacti species (*Opuntia spinosior*, *Opuntia engelmannii* and *Ferocactus wislizeni*). Similarly, watershed monitoring began in 1977 at the Jornada Experimental Range (JER), located 30 km north of Las Cruces, New Mexico, in the Chihuahuan Desert (Fig. 1), as described by Turnbull et al. (2013). Mean annual precipitation at the JER is considerably lower than SRER (251 mm/yr), with a similar proportion (53%) occurring during the summer monsoon (Templeton et al., 2014). Soils at the JER site are primarily sandy loam with high gravel contents (Anderson, 2013) transported from the San Andreas Mountains. The mixed shrubland ecosystem at the site consists of creosote bush (*Larrea tridentata*), honey mesquite (*Prosopis glandulosa* Torr.), several grass species (*Muhlenbergia porteri*, *Pleuraphis mutica* and *Sporobolus cryptandrus*), and other shrubs (*Parthenium incanum*, *Flourensia cernua* and *Gutierrezia sarothrae*). Fig. 2 presents a vegetation classification at each site grouped into major categories: (1) SRER has velvet mesquite (labeled mesquite), grasses, cacti (*Opuntia engelmannii* or prickly pear) and bare soil, while (2) JER has honey mesquite (labeled mesquite), creosote bush, other shrubs, grasses and bare soil. Table 1 presents the vegetation and terrain properties for the site watersheds obtained from 1-m digital elevation models (DEMs) and 1-m vegetation maps (Fig.

2). Pierini et al. (2014) and Templeton et al. (2014) describe the image acquisition and processing methods employed to derive these products at SRER and JER, respectively.

2.2. Distributed Sensor Networks at the Small Watershed Scale

Long-term watershed monitoring at the SRER and JER sites consisted of rainfall and runoff observations at Watersheds 7 and 8 (SRER, 1.25 ha) and the Tromble Weir (JER, 4.67 ha). Pierini et al. (2014) and Templeton et al. (2014) describe recent monitoring efforts using a network of rainfall, runoff, soil moisture and temperature observations, as well as radiation and energy balance measurements at EC towers, commencing in 2011 and 2010 at SRER and JER. This brief description of the distributed sensor networks is focused on the spatially-averaged measurements used for comparisons to the CRNS method. Precipitation (P) was measured using up to 4 tipping-bucket rain gauges (TE525MM, Texas Electronics) to construct a 30-min resolution spatial average based on Thiessen polygons within the watershed boundaries. At the watershed outlets, streamflow (Q) was estimated at Santa Rita supercritical runoff flumes (Smith et al., 1981) using a pressure transducer (CS450, Campbell Scientific Inc.) and an *in-situ* linear calibration to obtain 30-min resolution observations. Evapotranspiration (ET) was obtained at 30-min resolution using the EC technique that employs a three-dimensional sonic anemometer (CSAT3, Campbell Scientific Inc.) and an open path infrared gas analyzer (LI-7500, LI-COR Inc.) installed at 7-m height on each tower. Flux corrections for the EC measurements followed Scott et al. (2004) and were verified using an energy balance closure approach reported in Table 2 for the study period. Energy balance closure at both sites is within the reported values across a range of other locations where the ratio of $\Sigma(\lambda E + H)/\Sigma(R_n - G)$ has an average value of 0.8 (Wilson et al., 2002; Scott, 2010). To summarize these observations, Fig. 3 shows the spatially-averaged P, Q and ET (mm/hr), each aggregated to hourly resolution, at each study site during

March 1, 2013 to September 30, 2014, along with seasonal precipitation amounts. While the results compare favorably to previous measurements (Turnbull et al., 2013; Pierini et al., 2014; Templeton et al., 2014), it should be noted that *ET* and *Q* data are assumed to represent the spatially-averaged watershed conditions, despite the small mismatch between the watershed boundaries and EC footprints (Fig. 2) and the summation of *Q* in the two watersheds at SRER.

Distributed soil moisture measurements were obtained using soil dielectric probes (Hydra Probe, Stevens Water) organized as profiles (sensors placed at 5, 15 and 30 cm depths) in each study site. Profiles were originally installed at multiple locations along transects to investigate the different primary controls on soil moisture at each site: (1) at SRER, we installed four transects of 5 profiles each located under different vegetation classes (mesquite, grass, prickly pear and bare soil), and (2) at JER, we established three transects of 5 profiles each installed along different hillslopes (north-, south- and west-facing), as shown in Fig. 1. Individual sensors measure the impedance of an electric signal, as described in Campbell (1990), through a 40.3 cm^3 soil volume (5.7 cm in length and 3.0 cm in diameter) to determine the volumetric soil moisture (θ) in m^3/m^3 and soil temperature in ºC as 30-min averaged values. A 'loam' calibration equation was used in the conversion to θ (Seyfried et al., 2005) and corrected using relations established through gravimetric soil sampling at each study site (a power law relation at SRER with R^2 = 0.99 and a linear relation at JER with R^2 = 0.97), following Pierini (2013). Given that sensors were originally installed to conduct watershed studies, spatial averaging was performed using site-specific weighting schemes accounting for the main controls on the soil moisture distribution. Thus: (1) at SRER, we utilized the percentage area of each vegetation class (Table 1) and the associated sensor locations within each type (Pierini et al., 2014), and (2) at JER, we accounted for the aspect and elevation at the sensor locations and used these to extrapolate to other locations with similar characteristics based on the 1-m DEM (Templeton et al., 2014).

2.3. Cosmic-ray Neutron Sensing Method for Soil Moisture Estimation

The CRNS method relates soil moisture to the density of fast or moderated neutrons (Zreda et al., 2008) measured above the soil surface. A cosmic-ray neutron sensor (CRS-1000/B, Hydroinnova LLC) was installed in each watershed in January 2013 to record neutron counts at hourly intervals. We selected the study period (March 1, 2013 to September 30, 2014) to coincide with the availability of data from the distributed sensor networks. While the theory of using neutrons for soil moisture measurements has a long history (e.g., Gardner and Kirkham, 1952), recent developments in the measurement of neutrons generated from cosmic rays has increased the horizontal scale, reduced the need for manual sampling, and led to a non-invasive approach. Zreda et al. (2008) and Desilets and Zreda (2013) describe the horizontal scale as having a radius of ~300 m at sea level and a vertical aggregation scale ranging from 12 to 76 cm depending on soil wetness, while the work of Köhli et al. (2015) found a smaller horizontal scale with a radius of ~230 m at sea level. Since the travel speed of fast neutrons is >10 km/s, neutron mixing occurs almost instantaneously in the air above the soil surface (Glasstone and Edlund, 1952), providing a well-mixed region that can be sampled with a single detector.

Using a particle transport model, Desilets et al. (2010) found a theoretical relationship between the neutron count rate at a detector and soil moisture for homogeneous SiO_2 sand:

$$\theta(N) = \frac{0.0808}{\left(\frac{N}{N_o}\right) - 0.372} - 0.115 \quad , \qquad (1)$$

where θ (m^3/m^3) is volumetric soil moisture, N is the neutron count rate (counts/hr) normalized to the atmospheric pressure and solar activity level, and N_o (counts/hr) is the count rate over a dry soil under the same reference conditions. The corrections applied to the neutron count rate are detailed in Desilets and Zreda (2003) and Zreda et al. (2012) and are applied automatically in the COSMOS website (http://cosmos.hwr.arizona.edu/). Additionally, since neutron counts are affected by all sources of hydrogen in the support volume, we apply a correction (C_{WV}) for atmospheric water vapor that was derived by Rosolem et al. (2013) as:

$$C_{WV} = 1 + 0.0054\left(\rho_v^o - \rho_v^{ref}\right) \quad , \qquad (2)$$

where ρ_v^o (g/m^3) and ρ_v^{ref} (g/m^3) are absolute water vapors at current and reference conditions. To estimate N_o, we performed a manual soil sampling at 18 locations within the CRNS footprint (sampled every 60 degrees at radial distances of 25, 75 and 200 m from the detector) at 6 depths (0-5, 5-10, 10-15, 15-20, 20-25, 25-30 cm) for a total of 108 samples per site. Gravimetric soil moisture measurements were made following oven drying at 105 ºC for 48 hrs (Dane and Topp, 2002) and converted to volumetric soil moisture using the soil bulk density (1.54 ± 0.18 g/cm^3 at SRER and 1.3 ± 0.15 g/cm^3 at JER). The spatially-averaged volumetric soil moisture was related to the average neutron count obtained for the same time period (6-hr average) resulting in N_o = 3973 at SRER and N_o = 3944 at JER, considered to be in line with the expected amounts given the elevations of both sites. Table 3 compares the gravimetric measurements and the CRNS soil moisture estimates during the calibration dates and provides further details on the soil properties at the two sites. We applied a 12-hr boxcar filter to the measured count rates to remove the statistical noise associated with the measurement method (Zreda et al., 2012). On days where soil moisture changed by more than 0.06 m^3/m^3 due to rainfall, the boxcar filter was not applied. We note that additional terms to the calibration accounting for variations in lattice water, soil organic carbon and vegetation have been proposed (Zreda et al., 2012; Bogena et al., 2013; McJannet et al., 2014; Coopersmith et al. 2014). However, given the relatively small amount of biomass (~2.5

kg/m^2 at SRER, Huang et al., 2007; and ~0.5 kg/m^2 at JER, Huenneke et al., 2001), low soil organic carbon (4.2 mg C/g soil at SRER; and 2.7 mg C/g soil at JER, Throop et al., 2011), and low clay percent (5.2% at SRER; and 4.9% at JER, Anderson, 2013), and thus low lattice water amounts (Greacen, 1981), we have neglected these terms in the analysis. In addition, since a local calibration was performed, lattice water, biomass, and soil organic carbon are implicitly accounted for in the calculation of volumetric soil moisture from the calibration relation.

Fig. 2 presents the horizontal aggregation scale of the CRNS method in comparison to the watershed boundaries and to the EC footprints obtained for summer 2013 (Anderson, 2013). Since both the CRNS and EC footprints have horizontally-decaying contributions, we limited the size of the analysis region to the 50% contribution or source area to enhance the overlap with the watershed boundaries and sensor networks. The footprints for both the CRNS method and the EC method vary considerably (Anderson, 2013; Köhli et al., 2015), with temporal changes occurring in the amount of overlap with the watersheds and between each other. Nevertheless, the vegetation distributions sampled in the CRNS, EC, and watershed areas (Fig. 2) are nearly the same (Vivoni et al., 2014), and the soils have low spatial variability (Anderson, 2013; Table 3), such that CRNS and EC measurements are considered representative of the watershed conditions. In addition to the changing horizontal scale, the CRNS method measures a time-varying vertical scale that depends on the soil water content. Franz et al. (2012b) used a particle transport model to determine that the CRNS measurement depth, $z*$, varied with soil moisture as:

$$z^*(\theta) = \frac{5.8}{\rho_b \tau + \theta + 0.0829} \quad , \qquad (3)$$

where ρ_b is bulk density of the soil (Table 3) and τ is the weight fraction of lattice water in the mineral grains and bound water. Lattice water must be considered here since a local calibration of (3) is not possible. As a result, lattice water content was established at 0.02 g/g at each site given the weathered soils and the measurements from Franz et al. (2012b). To account for the temporal variation of z^*, the sensor profiles representing different soil layers (0-10 cm, 10-20 cm, and 20-40 cm in depth) were weighted based on z^* at each hourly time step according to:

$$wt(z) = a\left(1 - \left(\frac{z}{z^*}\right)^b\right) \qquad \text{for } 0 \leq wt \leq z^* \qquad , \qquad (4)$$

where $wt(z)$ is the weight at depth z, a is a constant defined to integrate the profile to unity ($a = 1/(z^* - \{z^{*b+1}/[z^{*b}(b + 1)]\})$), and b controls the shape of the weighting function. For simplicity, we assumed a value of $b = 1$ leading to a linear relationship (Franz et al., 2012b).

3. Methods

3.1. Comparison of CRNS to Distributed Network of Soil Moisture Sensors

The CRNS method was first validated against the distributed network of soil moisture sensors. As done in previous studies, we compared hourly soil moisture observations obtained from the CRNS method (θ_{CRNS}) to estimates from the distributed sensor network (θ_{SN}) that have been averaged in space (i.e., based on vegetation type at SRER and elevation/aspect location at JER) and depth-weighted according to the time-varying CRNS measurement depth (z^*). We used several metrics to quantitatively assess the comparisons, including Root Mean Square Error (RMSE), Correlation Coefficient (CC), Bias (B) and Standard Error of Estimates (SEE). We performed an additional test of the CRNS technique by comparing relations between the mean soil moisture ($<\theta>$), obtained from either θ_{CRNS} or θ_{SN}, and the spatial standard deviation (σ) of soil moisture measured in the distributed sensor network. This relation has been studied previously with the goal of evaluating the role of heterogeneities related to vegetation, terrain position and soil properties (Famiglietti et al., 1999; Lawrence and Hornberger, 2007; Fernández and Ceballos, 2003; Vivoni et al., 2008b; Mascaro et al., 2011; Qu et al., 2015). Based on Famiglietti et al. (2008), we fitted an empirical function to the observations at each site:

$$\sigma = k_1 \langle \theta \rangle e^{-k_2 \langle \theta \rangle} \tag{5}$$

where k_1 and k_2 are regression parameters, and compared these to prior studies in the region (e.g., Vivoni et al., 2008b; Mascaro and Vivoni, 2012; Stillman et al., 2014).

3.2. CRNS Water Balance Analyses Methods

In small watersheds of comparable size to the CRNS measurement footprint, the water balance can be expressed as:

$$z^* \frac{\Delta\theta}{\Delta t} = P - ET - Q - L \quad , \tag{6}$$

where $\Delta\theta$ is the change in volumetric soil moisture over the time interval Δt, P is precipitation, ET is evapotranspiration, Q is streamflow, and L is leakage or deep percolation, with all of the terms expressed as spatially-averaged quantities and valid over the effective soil measurement depth (z^*). The water balance was applied to validate the accuracy of the CRNS observations using measurements of the spatially-averaged fluxes (P, ET and Q) for a set of storm events. For each event, we computed the change in soil moisture measured by the CRNS, $\Delta\theta_{CRNS}$, and the change calculated from the water balance, $\Delta\theta_{WB}$. In both cases, changes were computed as the difference between the pre-storm soil moisture and the peak amount due to a rainfall event. For the application of (6), the soil measurement depth z^* was calculated as the average value over the duration of the soil moisture response to each individual storm. Note that, during a storm, ET is very low and the use of z^* in (6) instead of the plant rooting depth is justified. In addition, since this comparison is performed over a short time interval during the rising limb of the soil moisture response, we assumed no leakage (i.e., $L = 0$). To test the validity of this hypothesis, we analyzed the soil moisture records measured at the EC towers, where sensors were installed to measure the profile up to 1 m (i.e., a depth larger than z^*). We found that the percolation beyond a depth of ~40 cm is infrequent at both sites during summer monsoon storms, thus sustaining our assumption. However, percolation can occur on a time scale of several days during winter precipitation (e.g., Franz et al., 2012b; Templeton et al., 2014; Pierini et al., 2014). Although there are large amounts of bare soil in the watersheds, shrub and tree roots have been shown to extend laterally for 10 m or more (Heitschmidt et al., 1988), such that most of contributing area will be under the influence of both bare soil evaporation and plant transpiration.

Once validated against the distributed sensors and the application of the water balance, the CRNS estimates were subsequently used to determine the daily spatially-averaged fluxes into and out from the measurement depth (z^*) as proposed by Franz et al. (2012b):

$$f_{CRNS}(t) = \left(\theta_{CRNS,t} - \theta_{CRNS,t-1}\right)\min(z^*_t, z^*_{t-1}) / \Delta t \ . \qquad (7)$$

In (7), f_{CRNS} is the daily flux (mm/day), Δt is the time step (1 day), and $\min(z^*_t, z^*_{t-1})$ represents the minimum daily-averaged measurement depth between the two days being compared. Positive values of f_{CRNS} indicate an increase in soil moisture and, thus, represent net infiltration ($f_{CRNS} = I$) into the measurement depth, usually occurring after a rainfall event. As a result, assuming negligible plant interception, daily P data can be used to estimate Q as $P - I$, which in turn can be compared to the runoff measurements in the watersheds. On the other hand, negative values of f_{CRNS} are equal to the net outflow ($f_{CRNS} = O$), which can occur either as evapotranspiration or leakage. Using the EC method to obtain daily ET, $L = O - ET$ can be determined as a measure of exchanges between the soil layers above and below z^*: L is positive when there is drainage to deeper soil layers and negative when deeper water is being drawn to support plant transpiration.

3.3. Relation between Evapotranspiration and Soil Moisture at Commensurate Scale

Soil moisture at single locations is typically linked to ET in hydrologic models (e.g., Chen et al., 1996; Ivanov et al., 2004) and empirical studies (e.g., Small and Kurc, 2003; Vivoni et al., 2008a) using relations such as $ET = f(\theta)$. For example, a commonly used approach is based on a piecewise linear relation between daily ET and θ (Rodríguez-Iturbe and Porporato, 2004):

$$ET(\theta) = \begin{cases} 0 & 0 < \theta \le \theta_h \\ E_w \dfrac{\theta - \theta_h}{\theta_w - \theta_h} & \theta_h < \theta \le \theta_w \\ E_w + \left(ET_{\max} - E_w\right)\dfrac{\theta - \theta_h}{\theta^* - \theta_h} & \theta_w < \theta \le \theta^* \\ ET_{\max} & \theta^* < \theta \le \phi \end{cases}, \quad (8)$$

where E_w is soil evaporation, ET_{max} is maximum evapotranspiration, θ_h, θ_w, and θ^* are the hygroscopic, wilting and plant stress soil moisture thresholds, and ϕ is the soil porosity. Vivoni et al. (2008a) applied (8) to observations of ET from the EC method and θ at single locations to derive the relation parameters using a nonlinear optimization algorithm (Gill et al., 1981). We evaluate this approach using the spatially-averaged soil moisture estimates (θ_{CRNS} and θ_{SN}) whose spatial scale is more commensurate with the ET measurements than single measurement sites.

4. Results and Discussion

4.1. Comparison of CRNS Method to Distributed Sensor Network

Fig. 4 presents a comparison of the spatially-averaged, hourly soil moisture obtained from the CRNS method (θ_{CRNS}) and the distributed sensor network (θ_{SN}), as well as the time-varying measurement depth (z^*) of CRNS. Relative to the long-term summer precipitation (Table 1), the study period had below average (188 and 153 mm in 2013 and 2014) and significantly above average (246 and 247 mm) rainfall at SRER and JER, respectively. The fall-winter period in the record had below average precipitation (99 mm) at SRER and significantly below average amounts (21 mm) at JER. Overall, the spring periods were dry, consistent with the long-term averages. In response, the temporal variability of soil moisture clearly shows the seasonal conditions at the two sites, with relatively wetter conditions during the summer monsoons. Seasonally-averaged θ_{CRNS} compares favorably with seasonally-averaged θ_{SN} (Fig. 4), with both estimates showing relatively large differences between wetter summer conditions (0.065 and 0.085 m^3/m^3 at SRER and JER) and drier spring values (0.028 and 0.021 m^3/m^3 at SRER and JER, respectively). As shown in prior studies (e.g., Zreda et al., 2008; Franz et al., 2012b), the CRNS method tracks very well the sensor observations. Nevertheless, there is an indication that θ_{CRNS} has a tendency to dry less quickly during some rainfall events (i.e., overestimate soil moisture during recession limbs), possibly due to landscape features such as nearby channels (Fig. 1) and their associated zones of soil water convergence that remain wetter than areas measured by the distributed sensor network. Overall, however, there is an excellent match between θ_{CRNS} and θ_{SN} in terms of capturing the occurrence and magnitude of soil moisture peaks across the different seasons, thus reducing some issues noted by Franz et al. (2012b) with respect to a purported oversensitivity of θ_{CRNS} for small rainfall events (<5 mm). We attribute this improvement to the use of a 5 cm sensor in each profile that tracks important soil moisture dynamics occurring in the shallow surface layer within semiarid ecosystems.

To complement this, Fig. 5 compares θ_{CRNS} and θ_{SN} as a scatterplot along with the sample size (N) and the Standard Error of Estimates (SEE) which quantify the deviations from the 1:1 line. Table 4 provides the full set of statistical metrics for the comparison of θ_{CRNS} versus θ_{SN} at the two study sites. The correspondence between both methods is very good, with low RMSE and SEE, a high CC, and a Bias close to 1. These values are comparable to previous validation efforts where the RMSE was found to be 0.011 m^3/m^3 (Franz et al., 2012b) and less than 0.03

m^3/m^3 (Bogena et al., 2013; Coopersmith et al., 2014; Zhu et al., 2015). The comparison across the sites is also illustrative. Despite the more arid climate at JER (Table 1), the study period consisted of higher precipitation (247 mm) and higher soil moisture values during the summer (0.085 m^3/m^3), as compared to SRER (170 mm, 0.065 m^3/m^3), indicating a more active monsoon in the Chihuahuan Desert. In contrast, the fall-winter period is generally drier at JER (21 mm, 0.039 m^3/m^3), as compared to SRER (99 mm, 0.057 m^3/m^3), where high P and low ET in the winter promoted infiltration below the CRNS measurement depth, as observed at a 1-m sensor profile at SRER (not shown). These two effects lead to a larger range of soil moisture at JER as compared to SRER in Fig. 5. As a result, the CRNS method is found to be a reliable method for measuring soil moisture in the observed range of values at SRER and JER.

To further test the CRNS method against the distributed sensor network, Fig. 6 depicts the relations between the spatial variability of soil moisture (σ) and the spatially-averaged conditions ($<\theta>$). For illustration purposes, bin-averages and standard deviations are also presented for each relation. Least squares regressions of (5) based on hourly observations were applied to estimate k_1 and k_2 for the relations σ vs. θ_{SN} (k_1 = 0.75 and k_2 = 4.23 at SRER; k_1 = 0.74 and k_2 = 2.75 at JER) and these parameters were adopted to interpret the relations of σ vs. θ_{CRNS}. The RMSE are very low and similar in both cases (RMSE = 0.007 and 0.008 m^3/m^3 at SRER and 0.005 and 0.008 m^3/m^3 at JER for the relation with θ_{SN} and θ_{CRNS}, respectively), thus confirming the good correspondence between the two methods. As shown in prior efforts in semiarid ecosystems using sensor networks or aircraft observations (e.g., Fernández and Ceballos, 2003; Vivoni et al., 2008b; Mascaro et al., 2011; Stillman et al., 2014), there is a general increase in σ with $<\theta>$, explained by the role played by local heterogeneities (e.g., vegetation types, surface soil variations, topography) as well as the bounded nature of the soil moisture process at the driest state. The similar relations derived in these different sites might be broadly applicable to other semiarid ecosystems in the southwestern U.S.

4.2. Validation of CRNS Method with Water Balance Estimates

Fig. 7 presents the comparison of the spatially-averaged $\Delta\theta_{CRNS}$ and $\Delta\theta_{WB}$ as a scatterplot for approximately 40 rainfall events with a total depth larger than 10 mm and durations ranging from 0.5 to 31 hours (mean of 6 hours). The statistical metrics are presented in Table 4. The correspondence between the methods is very good, with low RMSE and SEE, a high CC, and a Bias close to 1, with a closer match at SRER. For example, the SEE at SRER (0.024 m^3/m^3) is significantly less than the value at JER (0.095 m^3/m^3) and close to the SEE of the comparison of θ_{CRNS} and θ_{SN}. This suggests that the three approaches (i.e., CRNS, sensor network, water balance) are in agreement at the SRER. For the JER, the lower correspondence between $\Delta\theta_{CRNS}$ and $\Delta\theta_{WB}$ is attributed to five large events where $\Delta\theta_{WB}$ is above 0.2 m^3/m^3. Removing these events lowers the SEE at JER to 0.020 m^3/m^3, in line with SRER and the comparison of θ_{CRNS} and θ_{SN} at JER. A closer inspection of the soil moisture response at JER allows investigating the physical reasons causing the different behavior of these five events. Fig. 8 shows the soil moisture change ($\Delta\theta_{SN}$) at different sensor depths averaged for the selected large events and for the remaining events, as well as the mean of CRNS measurement depths ($z*$) for each case. The five large events exhibit high soil moisture changes at 30 cm depth (i.e., 0.08 m^3/m^3) below $z*$ (i.e., 17 cm), while other events have soil moisture changes near zero at 30 cm and are captured well within $z*$. This indicates that infiltration fronts during the larger events penetrated beyond $z*$ and were not entirely captured by the CRNS method, leading to an underestimate of $\Delta\theta_{WB}$. For these events, the assumption L =0 in equation (6) is not fully supported. In contrast, the better correspondence at SRER suggests that infiltration fronts were contained within $z*$. This is plausible given the less rocky soil and flatter terrain at SRER as compared to JER (Anderson, 2013). At JER, soil water movement to deeper layers can be promoted by higher gravel contents and the presence of calcium carbonate and undulated terrain which facilitate lateral water transfer to channels with sandy bottoms (Templeton et al., 2014).

4.3. Utility of CRNS for Investigating Hydrological Processes

Given the confidence gained with respect to the CRNS estimates, we utilized these observations to quantify the water balance fluxes during storm and interstorm periods at the two sites. Fig. 9 shows the cumulative f_{CRNS} and the cumulative, spatially-averaged P and ET measured by the distributed sensor network. An overall drying trend is present at SRER during the study period (i.e., cumulative f_{CRNS} becomes more negative), while JER exhibits a relatively small change in cumulative f_{CRNS}, both in response to the below average (SRER) and above average (JER) precipitation. An important contrast at the sites is the overall water balance (Table 5), where higher P, lower ET, and lower Q at JER (measured ET/P = 0.54, Q/P = 0.01) implies that more soil water is available for leakage to deeper soil layers. This is reflected in a large positive difference between cumulative outflow ($O = ET + L$) and ET at JER (i.e., $L > 0$ from z^*, soil water movement to lower layers, as depicted in the soil water balance diagram). In contrast, SRER exhibits a higher ET/P = 0.96 and Q/P = 0.14, such that negative differences occur between O and ET (i.e., $L < 0$ into z^*, movement from lower layers, as depicted in the soil water balance diagram). This is particularly important during the summers when vegetation is active and produces more ET than the outflow from the CRNS measurement depth, indicating that soil water is obtained from deeper soil layers that are readily accessed by velvet mesquite roots (e.g., Snyder and Williams, 2003; Scott et al., 2008; Potts et al., 2010). This is consistent with the sustained *ET* during interstorm periods in the summer season at SRER despite the low θ_{CRNS}, while JER exhibits sharp declines in *ET* when θ_{CRNS} is reduced between storms.

Overall, the soil water balance from the CRNS method shows stark ecosystem differences at the two sites during the study period. The mesquite savanna at SRER extracted substantial amounts of water from deeper soil layers during the summer season such that losses to runoff and the atmosphere are in excess of seasonal precipitation. Deeper soil water is recharged beyond the CRNS measurement depth during winter periods, as observed by Scott et al., 2000, and subsequently accessed by deep-rooted trees during the summer (Scott et al., 2008). In contrast, the mixed shrubland at JER lost a substantial amount of precipitation to deeper soil layers throughout the year, due to the low values of runoff and evapotranspiration, and the soil, terrain and channel conditions promoting recharge (Templeton et al., 2014). Winter recharge is fostered by the lack of *ET* from drought-deciduous plants that lose their leaves in the wintertime. We hypothesize that deep percolation is likely occurring in the channels, since: (i) soil moisture observations in the hillslopes (i.e., far from the channel) show a lack of deep percolation, (ii) the runoff ratio decreases with the basin contributing area, indicating transmission losses along the channel (Templeton et al., 2014), and (iii) one sensor profile installed in a channel at SRER shows that the wetting front frequently reaches at least 30 cm depth. Furthermore, the f_{CRNS} approach provided estimates that can be compared to the watershed water balance since these are at a similar spatial scale (Table 5). Estimates of outflow (O) from the measurement depth and leakage (L) are higher when calculated with θ_{SN}, consistent with more rapid drying as compared to the CRNS method. On the other hand, the CRNS method results in higher values of the runoff ratio (Q/P) than observed in the distributed sensor network, in particular for JER. This is likely due to the daily scale of the CRNS analysis, which limits the suitability of the runoff estimate for semiarid watersheds characterized by runoff responses lasting minutes to hours.

4.4. Utility of CRNS for Improving *ET* Estimates

Fig. 10 compares the relationships between the measured daily *ET* using the EC method and the spatially-averaged soil moisture values (θ_{SN} and θ_{CRNS}) at the SRER and JER sites along with the piecewise linear regressions estimated using (8) and a nonlinear optimization approach. Following Vivoni et al. (2008a), regression parameters related to soil and vegetation conditions are presented in Table 6. For illustration purposes, bin-averages and standard deviations are also shown. Clearly, the piecewise linear relation is a suitable approach for capturing the ET-θ observations, yielding a relatively low RMSE at the two sites. A lower RMSE for the relation using θ_{CRNS} as compared to θ_{SN} at SRER is attributed to its ability to detect a wider range of dry conditions and the improved match in the spatial scales of *ET* and θ_{CRNS}, in an analogous fashion to the comparison between a single sensor and the distributed sensor network (Templeton et al., 2014). In addition, the CRNS method represents soil evaporation (E_w) in a more realistic way as it discriminates differences in drier states, illustrated by the realistic gradual increase of bare soil evaporation with increasing soil water (Fig. 10). For *ET* and θ_{SN}, the dry portions of the relations have too steep of a slope and do not represent well how bare soil evaporation changes with soil moisture. When comparing both sites through the ET-θ relation, the SRER has a larger E_w and ET_{max} and lower θ^*, as compared to JER, tested to be significantly different at the 95% confidence level using a bootstrap approach. Together, these parameters indicate that SRER has a higher overall *ET*, consistent with higher extractions from the CRNS measurement depth due to the mesquite trees, extensive grass cover and higher soil evaporation.

5. Summary and Conclusions

In this study, we utilized distributed sensor networks to examine the cosmic-ray neutron sensing soil moisture method at the small watershed scale in two semiarid ecosystems of the southwestern U.S. To our knowledge, this is the first study to compare CRNS measurements to two complementary approaches for obtaining spatially-averaged soil moisture at a commensurate scale: (1) a distributed set of sensor profiles weighted in the horizontal and vertical scales within each watershed, and (2) a watershed-averaged quantity obtained from closing the water balance. We highlighted a few novel advantages of the CRNS method revealed through the comparisons, including the ability to resolve the shallow soil moisture dynamics and to match the estimates obtained from closing the water balance for most rainfall events. In the distributed sensor comparisons, we found that the CRNS method overestimated soil moisture during the recession limbs of rainfall events, possibly due to landscape features such as nearby channels remaining wet. In the water balance comparisons, we identified that our assumption of no leakage beneath z^* was not met during large rainfall events and the CRNS method was not able to capture all of the soil water present. We attribute this to rapid bypassing of the measurement depth due to soil and terrain characteristics. Due to this observed bypass flow, we suggest that future studies using the CRNS method include a few soil moisture sensor profiles below z^* to detect leakage events.

The CRNS soil moisture estimates were used in combination with the various measurement methods to explore the relative magnitudes of the water balance components at each site given the different precipitation amounts during the study period. The drier than average conditions in the mesquite savanna ecosystem at SRER lead to drier surface soils incapable of supporting the measured evapotranspiration unless supplemented by plant water uptake from deeper soil layers. In contrast, wetter than average summer periods in the mixed shrubland at JER had wet surface soils that promoted leakage into the deeper vadose zone which was subsequently unavailable for runoff and evapotranspiration losses. Comparisons across different seasons also suggested that carryover of soil water from winter leakage toward deeper soil layers is consumed during the summer season by active plants. These novel inferences within the two ecosystems relied heavily on the application of the CRNS method and its limited measurement depth to discriminate between shallow and deeper vadose zone processes as well as on the direct measurement of the water balance components, in particular evapotranspiration. It is important to keep in mind, however, that the ability to resolve watershed-scale hydrological processes, such as the interaction between shallow and deep soil layers attributed to plant water uptake and leakage, depends to a large degree on the accuracy and representativeness of the distributed sensor network measurements and how their horizontal and vertical scales overlap with the CRNS measurement footprint. We expect these limitations to be especially critical in semiarid ecosystems with high spatial heterogeneity induced by vegetation and bare soil patches.

The collocation of a distributed sensor network within the CRNS measurement footprint also allowed us to examine important process-based relations that are often incorporated into hydrologic models or remote sensing analyses (e.g., Famiglietti and Wood, 1994; Famiglietti et al., 2008). The spatial variability of soil moisture is linked to the spatially-averaged conditions through predictable relations that do not vary significantly across the study sites. For higher mean soil moisture, we observed a nearly linear increase in spatial variability followed by an asymptotic behavior attributed to the seasonally-wet conditions during the North American monsoon. Based on these relations (k_1 and k_2), the spatial variability within a CRNS measurement footprint can be approximated for other semiarid ecosystems in the region. In addition, combining fixed and mobile CRNS methods can establish landscape scale (10^2 to 10^3

km^2) soil moisture monitoring networks at grid sizes (~1 km^2) comparable to land surface modeling (Franz et al., 2015). Similarly, intermediate scale soil moisture sensing can be linked effectively to daily evapotranspiration and used to obtain soil and vegetation parameters (E_w, ET_{max}, θ_h, θ_w, and θ^*) tailored to each ecosystem. In term of the ET-θ relation, the CRNS method has the potential to significantly improve land-atmosphere interaction studies through the commensurate scale achieved to the EC technique.

Acknowledgements

We thank three anonymous reviewers for their useful comments that helped to improve the manuscript. We also thank Mitch P. McClaran and Mark Heitlinger from the University of Arizona for help at the Santa Rita Experimental Range and John Anderson, Al Rango and other staff members at the USDA-ARS Jornada Experimental Range for their assistance. We thank funding from the U.S. Army Research Office (Grant 56059-EV-PCS) and the Jornada Long-Term Ecological Research project (National Science Foundation Grant DEB-1235828). We are also grateful to Nicole A. Pierini and Cody A. Anderson for help with field activities.

References

Alfieri, J.G., and Blanken, P.D.: How representative is a point? The spatial variability of surface energy fluxes across short distances in a sand-sagebrush ecosystem. Journal of Arid Environments, 87, 42-49, 2012.

Anderson, C.A.: Assessing land-atmosphere interactions through distributed footprint sampling at two eddy covariance towers in semiarid ecosystems of the southwestern U.S. Masters of Science in Civil, Environmental and Sustainable Engineering, Arizona State University, 243 pp., 2013.

Bartalis, Z., Wagner, W., Naeimi, V., Hasenauer, S., Scipal, K., Bonekamp, H., Figa, J., and Anderson, C.: Initial soil moisture retrievals from the METOP-A Advanced Scatterometer (ASCAT). Geophysical Research Letters, 34, L20401, 2007, doi: 10.1029/2007GL031088.

Bogena, H.R., Huisman, J.A., Baatz, R., Franssen, H.J.H., and Vereecken, H.: Accuracy of the cosmic-ray soil water content probe in humid forest ecosystems: The worst case scenario. Water Resources Research, 49(9), 5778-5791, 2013.

Browning, D.M., Franklin, J., Archer, S.R., Gillan, J.K., and Guertin, D.P.: Spatial patterns of grassland-shrubland state transitions: a 74-year record on grazed and protected areas. Ecological Applications, 24(6), 1421-1433, 2014.

Campbell, J.E.: Dielectric properties and influence of conductivity in soils at one to fifty Megahertz. Soil Science Society of America Journal, 54, 332-341, 1990.

Chen, F., Mitchell, K., Schaake, J., Xue, Y., Pan, H.-L., Koren, V., Duan, Q.Y., Ek, M., and Betts, A.: Modeling of land surface evaporation by four schemes and comparisons with FIFE observations. Journal of Geophysical Research, 101, 7251-7268, 1996.

Coopersmith, E.J., Cosh, M.H., and Daughtry, C.S.T.: Field-scale moisture estimates using COSMOS sensors: A validation study with temporary networks and Leaf-Area-Indices. Journal of Hydrology, 519, 637-643, 2014.

Dane, J.H., and Topp, C.G.: Methods of soil analysis. Part 4. Physical methods. SSSA Book Ser. 5. SSSA, Madison, WI, 2002.

Desilets, D., and Zreda, M.: Spatial and temporal distribution of secondary cosmic-ray nucleon intensities and applications to in-situ cosmogenic dating. Earth and Planetary Science Letters, 206, 21-42, 2003.

Desilets, D., and Zreda, M.: Footprint diameter for a cosmic-ray soil moisture probe: Theory and Monte Carlo simulations. Water Resources Research, 49, 3566-3575, 2013.

Desilets, D., Zreda, M., and Ferré, T.P.A.: Nature's neutron probe: Land surface hydrology at an elusive scale with cosmic rays. Water Resources Research, 46, W11505, 2010, doi:10.1029/2009WR008726.

Detto, M., Montaldo, N., Albertson, J.D., Mancini, M., and Katul, G.: Soil moisture and vegetation controls on evapotranspiration in a heterogeneous Mediterranean ecosystem on Sardinia, Italy. Water Resources Research, 42, W08419, 2006, doi:10.1029/2005WR004693.

Dugas, W.A., Hicks, R.A., and Gibbens, R.P.: Structure and function of C3 and C4 Chihuahuan Desert plant communities: Energy balance components. Journal of Arid Environments, 34, 63-79, 1996.

Eltahir, E.A.B.: A soil moisture rainfall feedback mechanism 1. Theory and observations. Water Resources Research, 34(4), 765-776, 1998.

Entekhabi, D.: Recent advances in land-atmosphere interaction research. Reviews of Geophysics, 33(S1), 995-1004, 1995.

Entekhabi, D., Njoku, E.G., O'Neill, P. E., Kellogg, K.H., Crow, W.T., Edelstein, W.N., Entin, J. K., Goodman, S.D., Jackson, T.J., Johnson, J., Kimball, J., Piepmeier, J.R., Koster, R.D., Martin, N., McDonald, K.C., Moghaddam, M., Moran, S., Reichle, R., Shi, J.C., Spencer, M.W., Thurman, S.W., Tsang, L., and Van Zyl, J.: The soil moisture active passive (SMAP) mission, Proceedings of the IEEE, 98, 704-716, 2010,

Falge, E., Baldocchi, D., Tenhunen, J., Aubinet, M., Bakwin, P., Berbigier, P., Bernhofer, C., Burba, G., Clement, R., Davis, K.J., Elbers, J.A., Goldstein, A.H., Grelle, A., Granier, A., Gudmundsson, J., Hollinger, D., Kowalski, A.S., Katul, G., Law, B.E., Malhi, Y., Meyers, T., Monson, R.K., Munger, J.W., Oechel, W., Paw, K.T., Pilegaard, K., Rannik, U., Rebmann, C., Suyker, A., Valentini, R., Wilson, K., and Wofsy, S.: Seasonality of ecosystem respiration and gross primary production as derived from FLUXNET measurements. Agricultural and Forest Meteorology, 113(1-4), 53-74, 2002.

Fernández, J.M., and Ceballos, A.: Temporal stability of soil moisture in a large-field experiment in Spain. Soil Science Society of America Journal, 67, 1647-1656, 2003.

Famiglietti, J.S., and Wood, E.F.: Multiscale modeling of spatially variable water and energy balance processes. Water Resources Research, 30, 3061-3078, 1994.

Famiglietti, J.S., Devereaux, J.A., Laymon, C.A., Tsegaye, T., Houser, P.R., Jackson, T.J., Graham, S.T., Rodell, M., and van Oevelen, P.J.: Ground-based investigation of soil moisture variability within remote sensing footprints during the Southern Great Plains 1997(SGP97) Hydrology Experiment. Water Resources Research, 35, 1839-1851, 1999.

Famiglietti, J. S., Ryu, D., Berg, A.A., Rodell, M., and Jackson, T.J.: Field observations of soil moisture variability across scales. Water Resources Research, 44, W01423, 2008, doi: 10.1029/2006WR005804.

Franz, T.E., Zreda, M., Ferré, T.P.A., Rosolem, R., Zweck, C., Stillman, S., Zeng, X., and Shuttleworth, W.J.: Measurement depth of the cosmic-ray soil moisture probe affected by hydrogen from various sources. Water Resources Research, 48, W08515, 2012a, doi:10.1029/2012WR011871.

Franz, T.E., Zreda, M., Rosolem, R., and Ferré, T.P.A.: Field validation of a cosmic-ray neutron sensor using a distributed sensor network. Vadose Zone Journal, 11(4), 2012b, doi: 10.2136/vzj2012.0046.

Franz, T.E., Zreda, M., Rosolem, R., Hornbuckle, B.K., Irvin, S.L., Adams, H., Kolb, T.E., Zweck, C., and Shuttleworth, W.J.: Ecosystem-scale measurements of biomass water using cosmic ray neutrons. Geophysical Research Letters, 40, 3929-3933, 2013a.

Franz, T.E., Zreda, M., Ferré, T.P.A., and Rosolem, R.: An assessment of the effect of horizontal soil moisture heterogeneity on the area-average measurement of cosmic-ray neutrons. Water Resources Research, 49, 6450-6458, 2013b.

Franz, T.E., Wang, T., Avery, W., Finkenbiner, C., and Brocca, L.: Combined analysis of soil moisture measurements from roving and fixed cosmic ray neutron probes for multiscale real-time monitoring. Geophysical Research Letters, 42, 2015, doi:10.1002/2015GL063963.

Gardner, W.H., and Kirkham, D.: Determination of soil moisture by neutron scattering. Soil Science, 73, 391-401, 1952.

Gibbens, R.P., and Beck, R.F.: Increase in number of dominant plants and dominance-classes on a grassland in the northern Chihuahuan Desert. Journal of Range Management, 40(2), 136-139, 1987.

Gill, P.E., Murray, W., and Wright, M.H.: Practical Optimization. Academic Press, London, UK, pp. 402, 1981.

Glasstone, S., and M. C. Edlund: Elements of Nuclear Reactor Theory, 416 pp., Van Nostrand, New York, 1952.

Greacen, E.L.: Soil Water Assessment by the Neutron Method, CSIRO, Melbourne, Australia, 148 pp., 1981.

Gutiérrez-Jurado, H.A., Vivoni, E.R., Cikoski, C., Harrison, J.B.J., Bras, R.L., and Istanbulluoglu, E.I.: On the observed ecohydrologic dynamics of a semiarid basin with aspect-delimited ecosystems. Water Resources Research, 49, 8263-8284, 2013.

Heitschmidt, R.K., Ansley, R.J., Dowhower, S.L., Jacoby, P.W., and Price, D.L.: Some observations from the excavation of honey mesquite root systems. Journal of Range Management, 41(3), 227-231, 1988.

Hsieh C.-I., Katul, G., and Chi, T.: An approximate analytical model for footprint estimation of scalar fluxes in thermally stratified atmospheric flows. Advances in Water Resources, 23, 765-772, 2000.

Huang, C., March, S.E., McClaran, M.P., and Archer, S.R.: Postfire stand structure in a semiarid savanna: cross-scale challenges estimating biomass. Ecological Applications, 17(7), 1899-1910, 2007.

Huenneke, L.F., Clason, D., and Muldavin, E.: Spatial heterogeneity in Chihuahuan Desert vegetation: implications for sampling methods in semi-arid ecosystems. Journal of Arid Environments, 47, 257-270, 2001.

Ivanov, V.Y., Vivoni, E.R., Bras, R.L., and Entekhabi, D.: Catchment hydrologic response with a fully-distributed triangulated irregular network model. Water Resources Research, 40, W11102, 2004, doi: 10.1029/2004WR003218.

Kerr, Y.H., Waldteufel, P., Wigneron, J.P., Martinuzzi, J.M., Font, J., and Berger, M.: Soil moisture retrieval from space: The Soil Moisture and Ocean Salinity (SMOS) mission. IEEE Transactions on Geoscience and Remote Sensing, 39, 1729-1735, 2001.

Köhli, M., Schrön, M., Zreda, M., Schmidt, U., Dietrich, P., and Zacharias, S.: Footprint characteristics revised for field-scale soil moisture monitoring with cosmic-ray neutrons. Water Resources Research, 51, 5772-5790, 2015.

Kormann, R., and Meixner, F.X.: An analytical footprint model for non-neutral stratification. Boundary Layer Meteorology, 99, 207-224, 2001.

Kustas, W.P., Zhan, X., and Schmugge, T.J.: Combining optical and microwave remote sensing for mapping energy fluxes in a semiarid watershed. Remote Sensing of Environment, 64, 116-131, 1998.

Laio, F., Porporato, A., Ridolfi, L., and Rodríguez-Iturbe, I.: Plants in water-controlled ecosystems: active role in hydrologic processes and response to water stress II. Probabilistic soil moisture dynamics. Advances in Water Resources, 24, 707-723, 2001.

Lawrence, J.E., and Hornberger, G.M.: Soil moisture variability across climate zones. Geophysical Research Letters, 34, L20402, 2007, doi: 10.1029/2007GL031382.

Mascaro, G., and Vivoni, E.R.: Utility of coarse and downscaled soil moisture products at L-band for hydrologic modeling at the catchment scale. Geophysical Research Letters, 39, L10403, 2012, doi: 10.1029/2012GL051809.

Mascaro, G., Vivoni, E.R., and Deidda, R.: Soil moisture downscaling across climate regions and its emergent properties. Journal of Geophysical Research, 116, D22114, 2011, doi: 10.1029/2011JD016231.

McJannet, D., Franz, T.E., Hawdon, A., Boadle, D., Baker, B., Almeida, A., Silberstein, R., Lambert, T., and Desilets, D.: Field testing of the universal calibration function for determination of soil moisture with cosmic-ray neutrons. Water Resources Research, 50(6), 5235-5248, 2014.

Moran, M.S., Hymer, D.C., Qi, J.G., and Sano, E.E.: Soil moisture evaluation using multi-temporal synthetic aperture radar (SAR) in semiarid rangeland. Agricultural and Forest Meteorology, 105, 69-80, 2000.

Narayan, U., and Lakshmi, V.: Characterizing subpixel variability of low resolution radiometer derived soil moisture using high resolution radar data. Water Resources Research, 44, W06425, 2008, doi:10.1029/2006WR005817.

Pierini, N.P., Vivoni, E.R., Robles-Morua, A., Scott, R.L., and Nearing, M.A.: Using observations and a distributed hydrologic model to explore runoff thresholds linked with mesquite encroachment in the Sonoran Desert. Water Resources Research, 50, 2014, doi: 10.1002/2014WR015781.

Pierini, N.A.: Exploring the ecohydrological impacts of woody plant encroachment in paired watersheds of the Sonoran Desert, Arizona. Master of Science Thesis in Civil, Environmental and Sustainable Engineering, Arizona State University, Tempe, AZ, 160 pp., 2013.

Polyakov, V.O., Nearing, M.A., Nichols, M.H., Scott, R.L., Stone, J.J., and McClaran, M.P.: Long-term runoff and sediment yields from small semiarid watersheds in southern Arizona. Water Resources Research, 46, W09512, 2010, 10.1029/2009WR009001.

Potts, D.L., Scott, R.S., Bayram, S., and Carbonara, J.: Woody plants modulate the temporal dynamics of soil moisture in a semi-arid mesquite savanna. Ecohydrology, 3, 20-27, 2010.

Qu, W., Bogena, H.R., Huisman, J.A., Vanderborght, J., Schuh, M., Priesack, E., and Vereecken, H.: Predicting sub-grid variability of soil water content from basic soil information. Geophysical Research Letters, 42, 789-796, 2015.

Rodríguez-Iturbe, I., and Porporato, A.: Ecohydrology of Water-Controlled Ecosystems, 442 pp., Cambridge Univ. Press, Cambridge, U.K., 2004.

Rosolem, R., Shuttleworth, W.J., Zreda, M., Franz, T., Zeng, X., and Kurc, S.A.: The effect of atmospheric water vapor on neutron count in the cosmic-ray soil moisture observing system. Journal of Hydrometeorology, 14, 1659-1671, 2013.

Scott, R.L., Shuttleworth, W.J., Keefer, T.O., and Warrick, A.W.: Modeling multi-year observations of soil moisture recharge in the semiarid American Southwest. Water Resources Research, 36(8), 2233-2247, 2000.

Scott, R.L.: Using watershed water balance to evaluate the accuracy of eddy covariance evaporation measurements for three semiarid ecosystems. Agricultural and Forest Meteorology, 150, 219-225, 2010.

Scott, R.L., Edwards, E.A., Shuttleworth, W.J., Huxman, T.E., Watts, C., and Goodrich, D.C.: Interannual and seasonal variation in fluxes of water and carbon dioxide from a riparian woodland ecosystem. Agricultural and Forest Meteorology, 122, 65-84, 2004.

Scott, R.L., Huxman, T.E., Williams, D.G., and Goodrich, D.C.: Ecohydrological impacts of woody-plant encroachment: seasonal patterns of water and carbon dioxide exchange within a semiarid riparian environment. Global Change Biology, 12, 311-324, 2006.

Scott, R.L., Cable, W.L., and Hultine, K.R.: The ecohydrologic significance of hydraulic redistribution in a semiarid savanna. Water Resources Research, 44, W02440, 2008, doi: 10.1029/2007WR006149.

Seyfried, M.S., Grant, L.E., Du, E., and Humes, K.: Dielectric loss and calibration of the Hydra probe soil water sensor. Vadose Zone Journal, 4, 1070-1079, 2005.

Small, E.E., and Kurc, S.A.: Tight coupling between soil moisture and the surface radiation budget in semiarid environments: Implications for land-atmosphere interactions. Water Resources Research, 39(10), 1278, 2003, doi: 10.1029/2002WR00129.

Smith, R.E., Chery, D.L., Renard, K.G., and Gwinn, W.R.: Supercritical flow flumes for measuring sediment-laden flow, Tech. Bull. 1655, 70 pp., U.S. Gov. Print. Off., Washington, D. C., 1981.

Snyder, K.A., and Williams, D.G.: Defoliation alters water uptake by deep and shallow roots of *Prosopis velutina* (velvet mesquite). Functional Ecology, 17, 363-374, 2003.

Stillman, S., Ninneman, J., Zeng, X., Franz, T., Scott, R.L., Shuttleworth, W.J., and Cummins, K.: Summer soil moisture spatiotemporal variability in southeastern Arizona. Journal of Hydrometeorology, 15(4), 1473-1485, 2014.

Templeton, R.C., Vivoni, E.R., Méndez-Barroso, L.A., Pierini, N.A., Anderson, C.A., Rango, A., Laliberte, A.S., and Scott, R.L.: High-resolution characterization of a semiarid watershed: Implications on evapotranspiration estimates. Journal of Hydrology, 509, 306-319, 2014.

Throop, H.L., Archer, S.R., Monger, H.C., and Waltman, S.: When bulk density methods matter: Implications for estimating soil organic carbon pools in rocky soils. Journal of Arid Environments, 77, 66-71, 2011.

Topp, G.C., Davis, J.L., and Annan, A.P.: Electromagnetic determination of soil water content: Measurements in coaxial transmission lines. Water Resources Research, 16(3), 574-582, 1980.

Turnbull, L., Parsons, A.J., and Wainwright, J.: Runoff responses to long-term rainfall variability in creosotebush-dominated shrubland. Journal of Arid Environments, 91, 88-94, 2013.

Vereecken, H., Huisman, J.A., Pachepsky, Y., Montzka, C., van der Kruk, J., Bogena, H., Weihermuller, L., Herbst, M., Martinez, G., and Vanderborght, J.: On the spatio-temporal dynamics of soil moisture at the field scale, Journal of Hydrology, 516, 76-96, 2014.

Vivoni, E.R., Moreno, H.A., Mascaro, G., Rodríguez, J.C., Watts, C.J., Garatuza-Payán, J., and Scott, R.L.: Observed relation between evapotranspiration and soil moisture in the North American monsoon region. Geophysical Research Letters, 35, L22403, 2008a, doi: 10.1029/2008GL036001.

Vivoni, E.R., Gebremichael, M., Watts, C.J., Bindlish, R., and Jackson, T.J.: Comparison of ground-based and remotely-sensed surface soil moisture estimates over complex terrain during SMEX04. Remote Sensing of Environment, 112(2), 314-325, 2008b.

Vivoni, E.R.: Spatial patterns, processes and predictions in ecohydrology: Integrating technologies to meet the challenge. Ecohydrology, 5(3), 235-241, 2012.

Vivoni, E.R., Watts, C.J., Rodriguez, J.C., Garatuza-Payan, J., Mendez-Barroso, L.A., and Saiz-Hernandez, J.A.: Improved land-atmosphere relations through distributed footprint sampling in a subtropical scrubland during the North American monsoon. Journal of Arid Environments, 74(5), 579-584, 2010.

Vivoni, E.R., Rango, A., Anderson, C.A., Pierini, N.A., Schreiner-McGraw, A.P., Saripalli, S., and Laliberte, A.S.: Ecohydrology with unmanned aerial vehicles. Ecosphere 5(10), art 130, 2014, http://dx.doi.org/10.1890/ES14-00217.1.

Western, A.W., Grayson, R.B., and Blöshl, G.: Scaling of soil moisture: A hydrologic perspective. Annual Review of Earth and Planetary Sciences, 30, 149-180, 2002.

Wilson, K., Goldstein, A., Falge, E., Aubinet, M., Baldocchi, D., Berbigier, P., Bernhofer, C., Ceulemans, R., Dolman, H., Field, C., Grelle, A., Ibrom, A., Law, B.E., Kowalski, A., Meyers, T., Moncrieff, J., Monson, R., Oechel, W., Tenhunen, J., Valentini, R., and Verma, S.: Energy balance closure at FLUXNET sites. Agricultural and Forest Meteorology, 113, 223-243, 2002.

Zhu, Z., Tan, L., Gao, S., and Jiao, Q.: Observation on soil moisture of irrigation cropland by cosmic-ray probe. IEEE Geoscience and Remote Sensing Letters, 12(3), 2015, doi: 10.1109/LGRS.2014.2346784.

Zreda, M., Desilets, D., Ferre, T.P.A., and Scott, R.L.: Measuring soil moisture content non-invasively at intermediate spatial scale using cosmic-ray neutrons. Geophysical Research Letters, 35, L21402, 2008, doi: 10.1029/2008GL035655.

Zreda, M., Shuttleworth, W.J., Zeng, X., Zweck, C., Desilets, D., Franz, T., and Rosolem, R.: COSMOS: the Cosmic-ray Soil Moisture Observing System. Hydrology and Earth System Sciences, 16, 4079-4099, 2012.

Figure Captions

Fig. 1: (a) Location of the study sites in Arizona and New Mexico. Watershed representations and sensor locations at (b) SRER and (c) JER, shown at the same scale.

Fig. 2: Vegetation classification for (a) SRER and (b) JER derived from aerial image analyses along with sensor locations and the 50% contributing areas of the CRNS and EC footprints.

Fig. 3: Hourly precipitation, streamflow and evapotranspiration at the (a) SRER and (b) JER sites during the study period (March 2013 to September 2014). Gaps in *ET* data indicate periods of EC tower malfunction due to equipment failures, data collection problems or vandalism. Vertical dashed lines indicate the seasonal definitions and their corresponding total precipitation.

Fig. 4: Comparison of the spatially-averaged, hourly soil moisture (m^3/m^3) from CRNS method (θ_{CRNS}, black lines) and distributed sensor network (θ_{SN}, gray lines) at (a) SRER and (b) JER, along with spatially-averaged, hourly precipitation during March 1, 2013 to September 30, 2014. Vertical dashed lines indicate the seasonal definitions and their corresponding seasonally-averaged θ_{CRNS} and θ_{SN} in m^3/m^3. Also shown are the time-varying measurement depths (z^*).

Fig. 5: Scatterplots of the spatially-averaged, hourly soil moisture (m^3/m^3) from CRNS method (θ_{CRNS}) and distributed sensor network (θ_{SN}) at (a) SRER and (b) JER. The SEE and the number of hourly samples (N) are shown for each site. Bin averages and ±1 standard deviation are shown (circles and error bars) for bin widths of 0.025 m^3/m^3.

Fig. 6: Soil moisture spatial variability as a function of the spatially-averaged distributed sensor network (θ_{SN}, top) and the CRNS method (θ_{CRNS}, bottom) for (a, c) SRER and (b, d) JER. Bin averages and ±1 standard deviation are shown (circles and error bars) for bin widths of 0.015

m^3/m^3 at SRER and 0.025 m^3/m^3 at JER. Regressions for the relations of σ with $<\theta>$ are valid for the entire dataset.

Fig. 7: Scatterplots of the spatially-averaged change in soil moisture (m^3/m^3) derived from CRNS method ($\Delta\theta_{CRNS}$) and the application of the water balance ($\Delta\theta_{WB}$) at (a) SRER and (b) JER. The SEE and the number of event samples (N) are shown for each site.

Fig. 8: Change in soil moisture ($\Delta\theta_{SN}$) at depths of 5, 15 and 30 cm at the JER for the five large events (‘Selected Events’) and the remaining cases (‘Other Events’). Horizontal lines are the time-averaged CRNS measurement depths averaged over Selected Events (black; standard deviation of 3.8 cm) and Other Events (gray; standard deviation of 6.5 cm).

Fig. 9: Comparison of cumulative f_{CRNS} and measured water balance fluxes (P and ET) during study period. CRNS estimates of infiltration (I), outflow (O) and leakage (L) are either depicted as cumulative fluxes ($O = ET + L$) or as total amounts during the study period (I and L) as arrows in the soil water balance box of depth z*. Shaded regions indicate the summer seasons (July-September). The horizontal line represents $f_{CRNS} = 0$.

Fig. 10: Evapotranspiration relation with the spatially-averaged distributed sensor network (θ_{SN}, top) and the CRNS method (θ_{CRNS}, bottom) for (a, c) SRER and (b, d) JER. Bin averages and ±1 standard deviation are shown (circles and error bars) for bin widths of 0.015 m^3/m^3 at SRER and 0.025 m^3/m^3 at JER. Regressions for the relations of ET with $<\theta>$ are valid for the entire dataset.

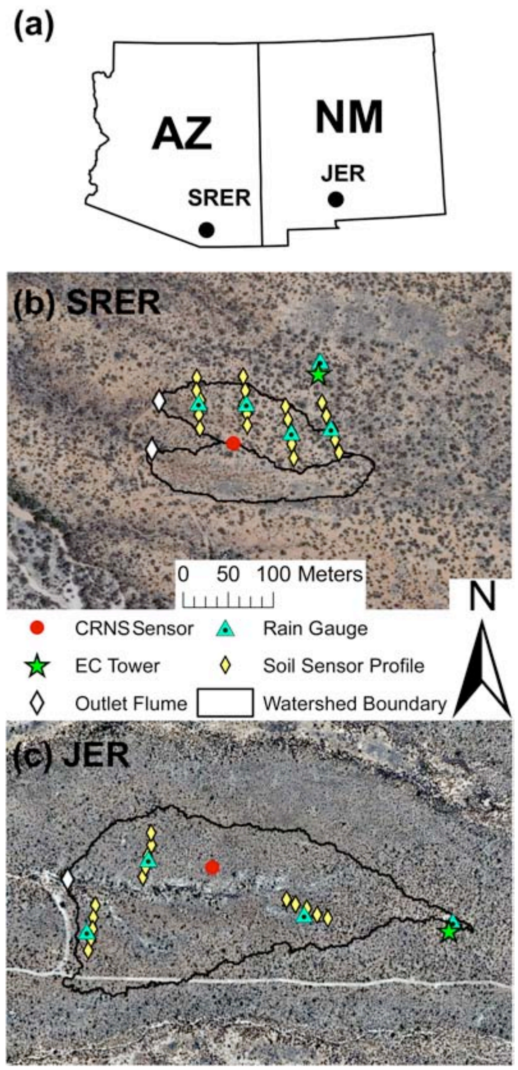

Fig. 1: (a) Location of the study sites in Arizona and New Mexico. Watershed representations and sensor locations at (b) SRER and (c) JER, shown at the same scale.

(Schreiner-McGraw et al., 2015, Fig. 1)

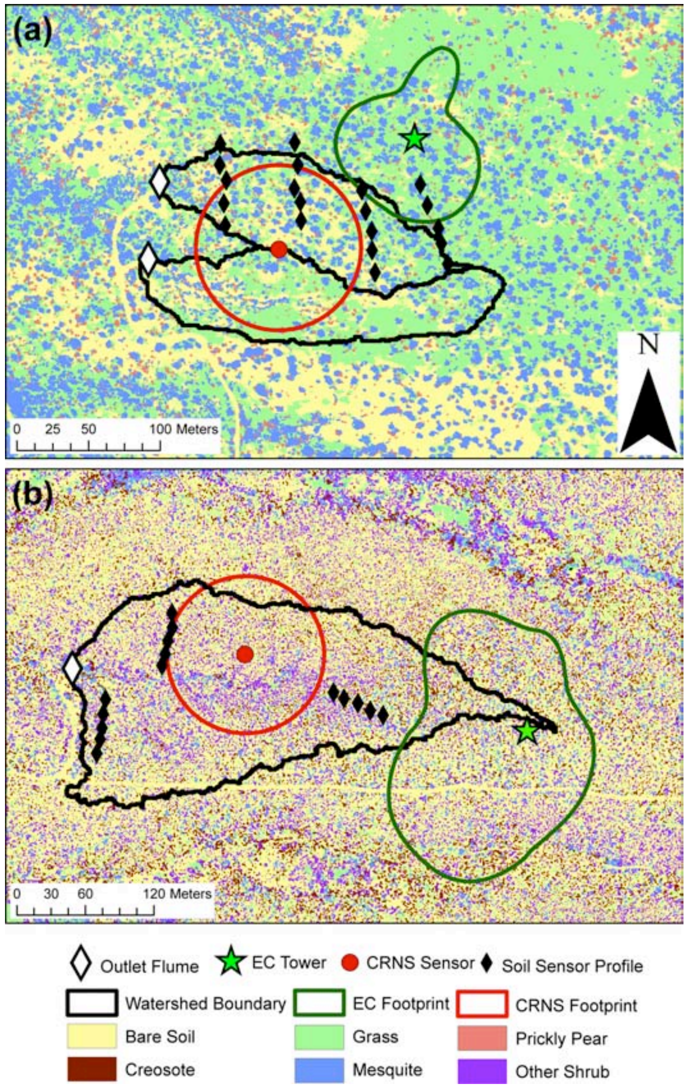

Fig. 2: Vegetation classification for (a) SRER and (b) JER derived from aerial image analyses along with sensor locations and the 50% contributing areas of the CRNS and EC footprints.

(Schreiner-McGraw et al., 2015, Fig. 2)

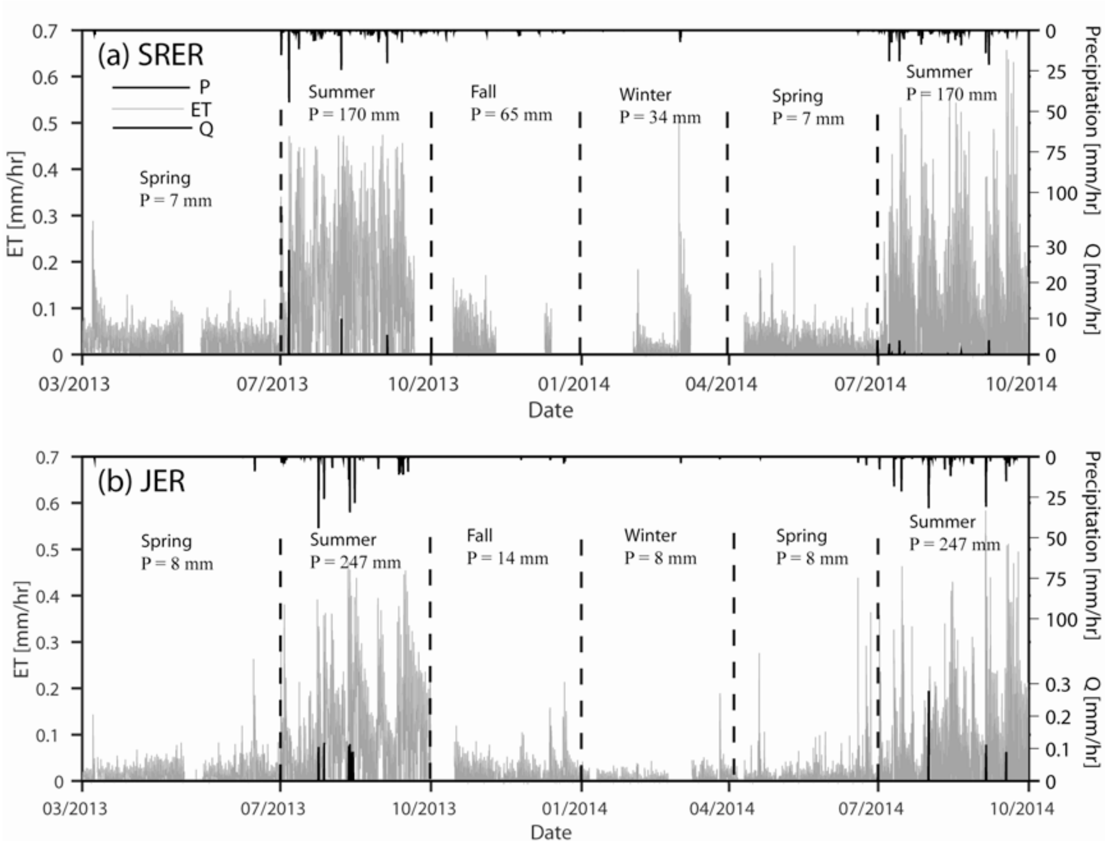

Fig. 3: Hourly precipitation, streamflow and evapotranspiration at the (a) SRER and (b) JER sites during the study period (March 2013 to September 2014). Gaps in *ET* data indicate periods of EC tower malfunction due to equipment failures, data collection problems or vandalism. Vertical dashed lines indicate the seasonal definitions and their corresponding total precipitation.

(Schreiner-McGraw et al., 2015, Fig. 3)

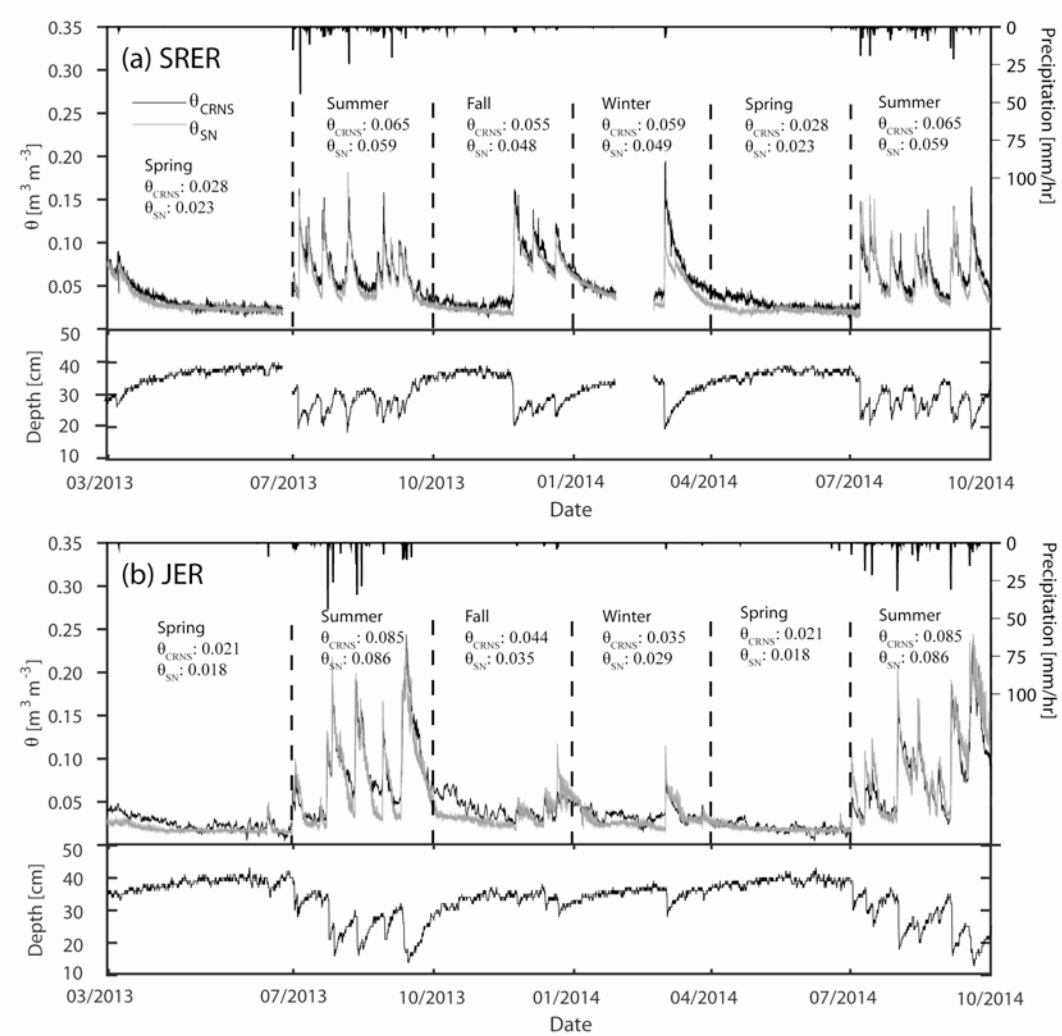

Fig. 4: Comparison of the spatially-averaged, hourly soil moisture (m^3/m^3) from CRNS method (θ_{CRNS}, black lines) and distributed sensor network (θ_{SN}, gray lines) at (a) SRER and (b) JER, along with spatially-averaged, hourly precipitation during March 1, 2013 to September 30, 2014. Vertical dashed lines indicate the seasonal definitions and their corresponding seasonally-averaged θ_{CRNS} and θ_{SN} in m^3/m^3. Also shown are the time-varying measurement depths (z^*).

(Schreiner-McGraw et al., 2015, Fig. 4)

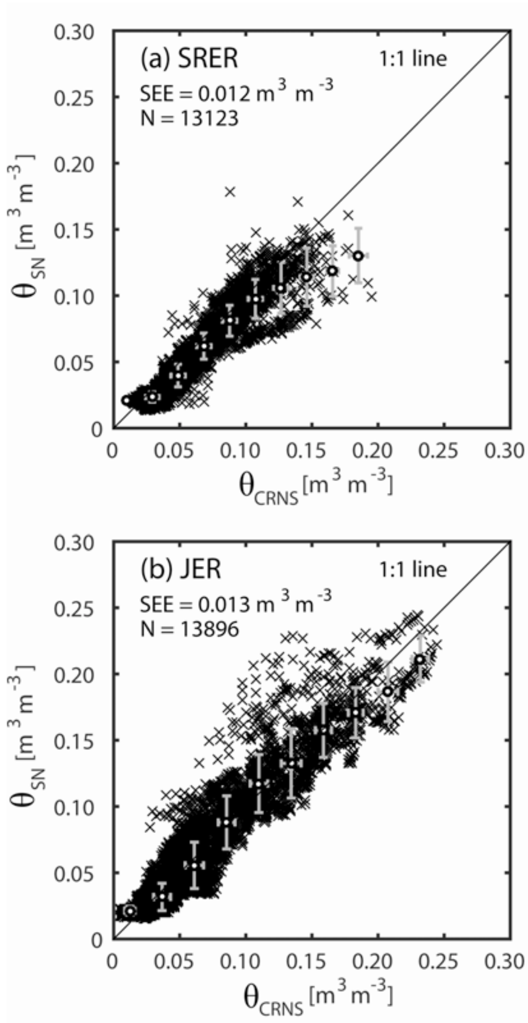

Fig. 5: Scatterplots of the spatially-averaged, hourly soil moisture (m^3/m^3) from CRNS method (θ_{CRNS}) and distributed sensor network (θ_{SN}) at (a) SRER and (b) JER. The SEE and the number of hourly samples (N) are shown for each site. Bin averages and ±1 standard deviation are shown (circles and error bars) for bin widths of 0.025 m^3/m^3.

(Schreiner-McGraw et al., 2015, Fig. 5)

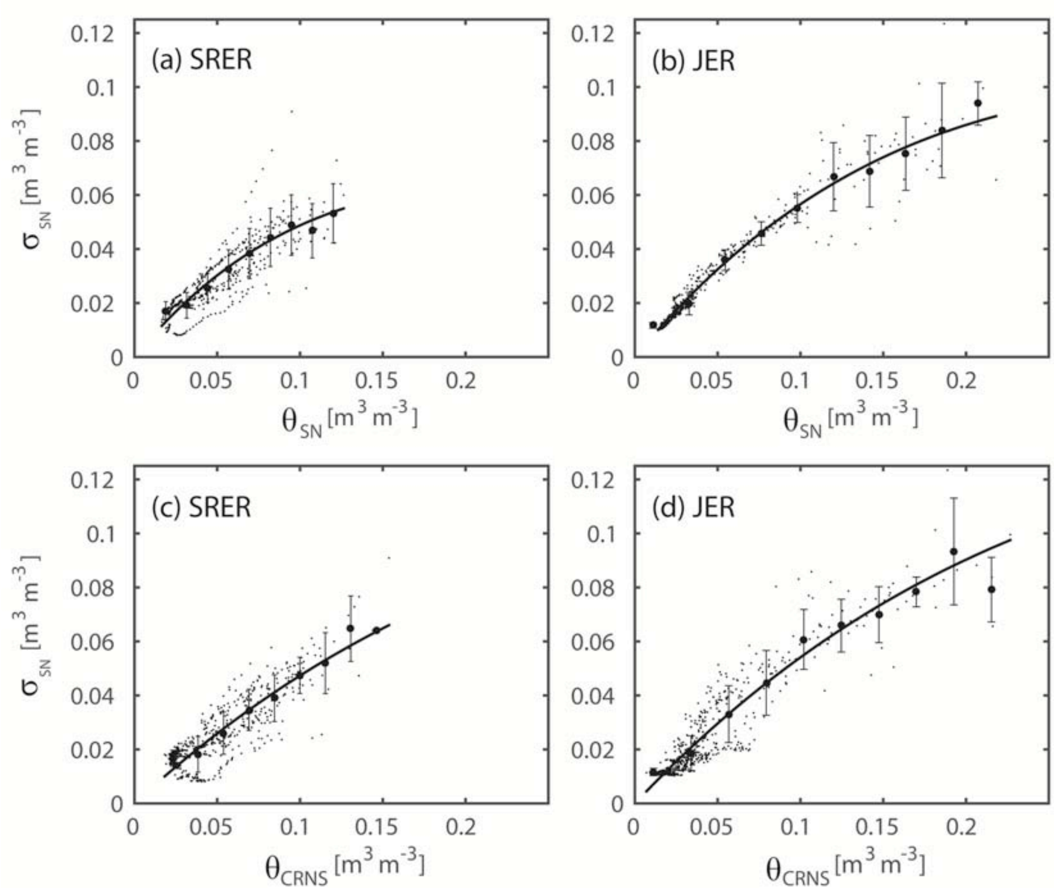

Fig. 6: Soil moisture spatial variability as a function of the spatially-averaged distributed sensor network (θ_{SN}, top) and the CRNS method (θ_{CRNS}, bottom) for (a, c) SRER and (b, d) JER. Bin averages and ±1 standard deviation are shown (circles and error bars) for bin widths of 0.015 m^3/m^3 at SRER and 0.025 m^3/m^3 at JER. Regressions for the relations of σ with $<\theta>$ are valid for the entire dataset.

(Schreiner-McGraw et al., 2015, Fig. 6)

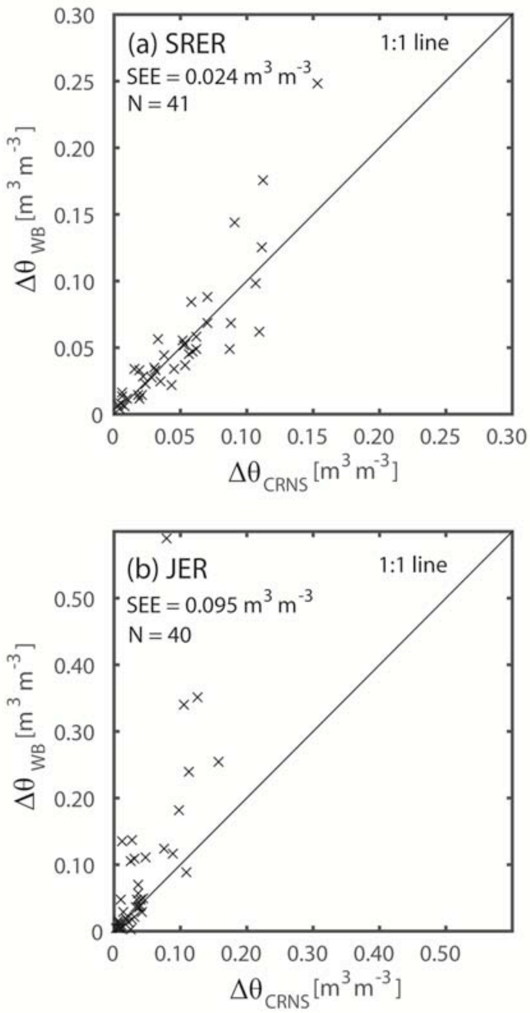

Fig. 7: Scatterplots of the spatially-averaged change in soil moisture (m^3/m^3) derived from CRNS method ($\Delta\theta_{CRNS}$) and the application of the water balance ($\Delta\theta_{WB}$) at (a) SRER and (b) JER. The SEE and the number of event samples (N) are shown for each site.

(Schreiner-McGraw et al., 2015, Fig. 7)

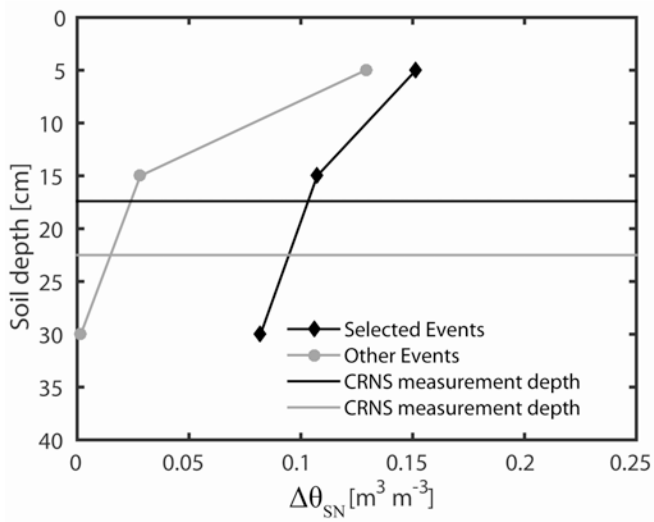

Fig. 8: Change in soil moisture ($\Delta\theta_{SN}$) at depths of 5, 15 and 30 cm at the JER for the five large events ('Selected Events') and the remaining cases ('Other Events'). Horizontal lines are the time-averaged CRNS measurement depths averaged over Selected Events (black, standard deviation of 3.8 cm) and Other Events (gray, standard deviation of 6.5 cm).

(Schreiner-McGraw et al., 2015, Fig. 8)

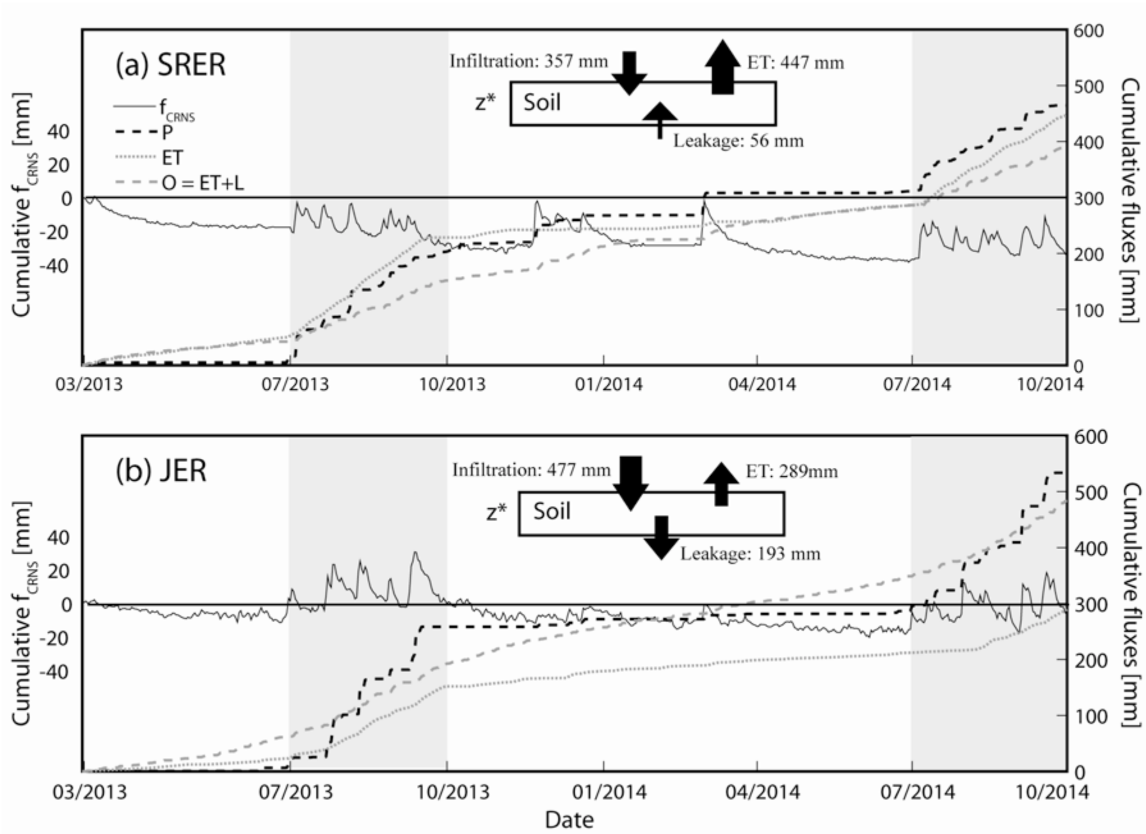

Fig. 9: Comparison of cumulative f_{CRNS} and measured water balance fluxes (P and ET) during study period. CRNS estimates of infiltration (I), outflow (O) and leakage (L) are either depicted as cumulative fluxes ($O = ET + L$) or as total amounts during the study period (I and L) as arrows in the soil water balance box of depth $z*$. Shaded regions indicate the summer seasons (July-September). The horizontal line represents $f_{CRNS} = 0$.

(Schreiner-McGraw et al., 2015, Fig. 9)

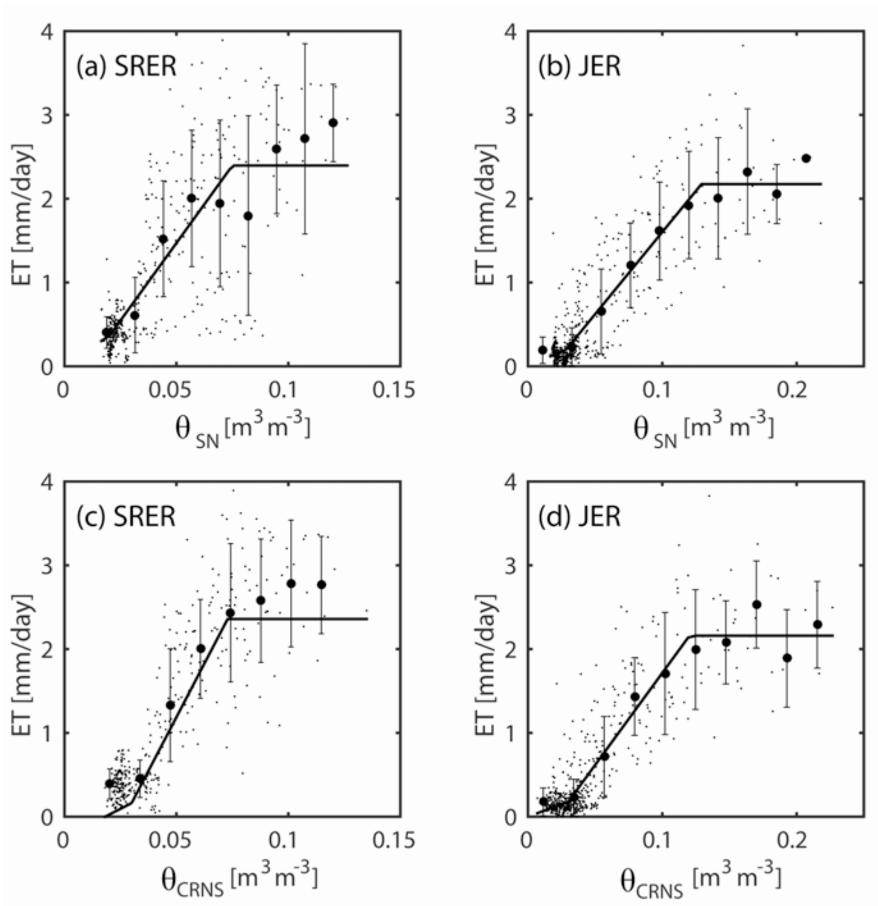

Fig. 10: Evapotranspiration relation with the spatially-averaged distributed sensor network (θ_{SN}, top) and the CRNS method (θ_{CRNS}, bottom) for (a, c) SRER and (b, d) JER. Bin averages and ±1 standard deviation are shown (circles and error bars) for bin widths of 0.015 m^3/m^3 at SRER and 0.025 m^3/m^3 at JER. Regressions for the relations of *ET* with <θ> are valid for the entire dataset.

(Schreiner-McGraw et al., 2015, Fig. 10)

Table Captions

Table 1: Watershed and precipitation characteristics at the SRER and JER sites. Precipitation values are long-term averages (1923-2014 at SRER and 1915-2006 at JER) for annual and seasonal quantities, defined as fall (October-December), winter (January-March), spring (April-June) and summer (July-September).

Table 2: Energy balance closure at SRER and JER using 30-min net radiation (R_n), ground (G), latent (λE) and sensible (H) heat fluxes. The parameters m and b are the slope and intercept in the relation $\lambda E + H = m(R_n - G) + b$, while the ratio of the sum of ($\lambda E + H$) to the sum of ($R_n - G$) is a measure of how much available energy is accounted for in the turbulent fluxes.

Table 3: Soil properties at SRER and JER. Soil moisture values correspond to conditions during the CRNS calibration dates (February 13, 2013 at SRER and February 10, 2013 at JER) for the gravimetric sampling at 18 locations with six depths (θ_G), CRNS (θ_{CRNS}) and the sensor network (θ_{SN}), each expressed as volumetric soil moisture using the soil bulk density (ρ_b) and soil porosity (ϕ) of the samples. Mean values of θ_G, ρ_b and ϕ are shown along with the ± 1 standard deviations. Particle size distributions were obtained from soil auger sampling of the top 45 cm at 20 locations at each site (Anderson, 2013). Mean values of percent clay, silt, sand and gravel are shown along with the ± 1 standard deviations.

Table 4: Statistical comparisons of CRNS method with distributed sensor network and water balance estimates based on the Standard Error of Estimates (SEE), Root Mean Square Error (RMSE), Bias (B), and Correlation Coefficient (CC), described in Vivoni et al. (2008b). Values in parentheses for JER indicate metrics when large rainfall events are excluded.

Table 5: Total water flux estimates from daily CRNS soil water balance method (f_{CRNS}) and daily sensor measurements during study period at the SRER and JER sites. P is from rain gauge measurements in both cases. L in CRNS is computed as $O - ET$ where ET is from EC method, while L in sensor estimates is calculated from solving the water balance.

Table 6: Regression parameters for the relations of evapotranspiration and soil moisture (θ_{SN} and θ_{CRNS}) at the SRER and JER sites along with the RMSE of the regressions. $\theta_h = 0$ in all cases.

Characteristic (unit)	Value	SRER	JER
Watershed area (m^2)		12535	46734
Elevation (m)	mean	1166.6	1458.3
	max	1171.1	1467.5
	min	1160.9	1450.5
Slope (degree)	mean	3.2	3.9
	max	19.2	45
	min	2.1	0
Drainage density (1/m)		0.04	0.03
Major vegetation type (%)	shrubs	32%	27%
	cacti	6%	1%
	grasses	37%	6%
	bare soil	25%	66%
Precipitation (mm)	annual	364	251
	fall	72	54
	winter	69	31
	spring	26	32
	summer	197	134

Table 1: Watershed and precipitation characteristics at the SRER and JER sites. Precipitation values are long-term averages (1923-2014 at SRER and 1915-2006 at JER) for annual and seasonal quantities, defined as fall (October-December), winter (January-March), spring (April-June) and summer (July-September).

(Schreiner-McGraw et al., 2015, Table 1)

Site	$\lambda E + H = m(R_n - G) + b$		$\frac{\sum \lambda E + H}{\sum R_n - G}$
	m	***b***	
SRER	0.72	17	0.85
JER	0.72	9.9	0.82

Table 2: Energy balance closure at SRER and JER using 30-min net radiation (R_n), ground (G), latent (λE) and sensible (H) heat fluxes. The parameters m and b are the slope and intercept in the relation $\lambda E + H = m(R_n - G) + b$, while the ratio of the sum of ($\lambda E + H$) to the sum of ($R_n - G$) is a measure of how much available energy is accounted for in the turbulent fluxes.

(Schreiner-McGraw et al., 2015, Table 2)

Property (unit)	SRER	JER
Soil Moisture Calibration		
θ_G (m^3/m^3)	0.114 ± 0.023	0.056 ± 0.013
θ_{CRNS} (m^3/m^3)	0.114	0.056
θ_{SN} (m^3/m^3)	0.105	0.016
ρ_b (g/cm^3)	1.54 ± 0.18	1.30 ± 0.15
ϕ (m^3/m^3)	0.42 ± 0.07	0.51 ± 0.06
Particle Size Distribution		
Clay (%)	5.2 ± 1.3 %	4.9 ± 1.1 %
Silt (%)	13.0 ± 2.2 %	28.5 ± 5.0 %
Sand (%)	72.5 ± 5.7 %	34.9 ± 8.3 %
Gravel (%)	9.3 ± 5.1 %	34.7 ± 11.5 %

Table 3: Soil properties at SRER and JER. Soil moisture values correspond to conditions during the CRNS calibration dates (February 13, 2013 at SRER and February 10, 2013 at JER) for the gravimetric sampling at 18 locations with six depths (θ_G), CRNS (θ_{CRNS}) and the sensor network (θ_{SN}), each expressed as volumetric soil moisture using the soil bulk density (ρ_b) and soil porosity (ϕ) of the samples. Mean values of θ_G, ρ_b and ϕ are shown along with the ± 1 standard deviations. Particle size distributions were obtained from soil auger sampling of the top 45 cm at 20 locations at each site (Anderson, 2013). Mean values of percent clay, silt, sand and gravel are shown along with the ± 1 standard deviations.

(Schreiner-McGraw et al., 2015, Table 3)

Metric (unit)	SRER	JER
θ_{CRNS} versus θ_{SN}		
RMSE (m^3/m^3)	0.009	0.013
CC	0.949	0.946
B	1.117	1.019
SEE (m^3/m^3)	0.012	0.013
$\Delta\theta_{CRNS}$ versus $\Delta\theta_{WB}$		
RMSE (m^3/m^3)	0.001	0.082 (0.019)
CC	0.949	0.940 (0.945)
B	0.936	0.543 (0.903)
SEE (m^3/m^3)	0.024	0.095 (0.020)

Table 4: Statistical comparisons of CRNS method with distributed sensor network and water balance estimates based on the Standard Error of Estimates (SEE), Root Mean Square Error (RMSE), Bias (B), and Correlation Coefficient (CC), described in Vivoni et al. (2008b). Values in parentheses for JER indicate metrics when large rainfall events are excluded.

(Schreiner-McGraw et al., 2015, Table 4)

Water Flux	SRER	JER
CRNS Estimates		
Precipitation (*P*, mm)	464	533
Infiltration (*I*, mm)	357	477
Outflow (*O*, mm)	391	482
Leakage (*L*, mm)	-56	193
Outflow ratio (*O*/*P*)	0.84	0.90
Runoff ratio (*Q*/*P*)	0.23	0.11
Sensor Measurements		
Precipitation (*P*, mm)	464	533
Storage change ($\Delta\theta$, mm)	-13	26
Outflow (*O*, mm)	437	506
Leakage (*L*, mm)	-10	217
Evapotranspiration (*ET*, mm)	447	289
Evaporation ratio (*ET*/*P*)	0.96	0.54
Streamflow (*Q*, mm)	64	5
Runoff ratio (*Q*/*P*)	0.14	0.01

Table 5: Total water flux estimates from daily CRNS soil water balance method (f_{CRNS}) and daily sensor measurements during study period at the SRER and JER sites. *P* is from rain gauge measurements in both cases. *L* in CRNS is computed as *O* – *ET* where *ET* is from EC method, while *L* in sensor estimates is calculated from solving the water balance.

(Schreiner-McGraw et al., 2015, Table 5)

Site	Relation	ET_{max} (mm/day)	E_w (mm/day)	θ_w (m^3/m^3)	θ^* (m^3/m^3)	RMSE (mm/day)
SRER	ET - θ_{SN}	2.61	0.41	0.03	0.07	1.15
	ET - θ_{CRNS}	2.40	0.36	0.02	0.08	0.55
JER	ET - θ_{SN}	2.16	0.18	0.03	0.12	0.34
	ET - θ_{CRNS}	2.17	0.21	0.03	0.13	0.34

Table 6: Regression parameters for the relations of evapotranspiration and soil moisture (θ_{SN} and θ_{CRNS}) at the SRER and JER sites along with the RMSE of the regressions. θ_h = 0 in all cases.

(Schreiner-McGraw et al., 2015, Table 6)